Ultraviolet refractometry using field-based light scattering spectroscopy

Dan Fu,[1] Wonshik Choi,[1,2,*] Yongjin Sung,[1] Seungeun Oh,[1] Zahid Yaqoob,[1] Yongkeun Park,[1] Ramachandra R. Dasari,[1] and Michael S. Feld[1]

[1]G. R. Harrison Spectroscopy Laboratory, Massachusetts Institute of Technology. Cambridge, Massachusetts 02139, USA

[2]Department of Physics, Korea University, Seoul 136-701, Korea

**wonshik@mit.edu*

Abstract: Accurate refractive index measurement in the deep ultraviolet (UV) range is important for the separate quantification of biomolecules such as proteins and DNA in biology. This task is demanding and has not been fully exploited so far. Here we report a new method of measuring refractive index using field-based light scattering spectroscopy, which is applicable to any wavelength range and suitable for both solutions and homogenous objects with well-defined shape such as microspheres. The angular scattering distribution of single microspheres immersed in homogeneous media is measured over the wavelength range 260 to 315 nm using quantitative phase microscopy. By least square fitting the observed scattering distribution with Mie scattering theory, the refractive index of either the sphere or the immersion medium can be determined provided that one is known *a priori*. Using this method, we have measured the refractive index dispersion of SiO_2 spheres and bovine serum albumin (BSA) solutions in the deep UV region. Specific refractive index increments of BSA are also extracted. Typical accuracy of the present refractive index technique is ≤0.003. The precision of refractive index measurements is ≤0.002 and that of specific refractive index increment determination is ≤0.01 mL/g.

OCIS codes: (120.3180) Interferometry; (180.0180) Microscopy; (170.3880) Medical and biological imaging.

References and Links

1. A. Barty, K. A. Nugent, D. Paganin, and A. Roberts, "Quantitative optical phase microscopy," Opt. Lett. **23**(11), 817–819 (1998).
2. B. Rappaz, P. Marquet, E. Cuche, Y. Emery, C. Depeursinge, and P. Magistretti, "Measurement of the integral refractive index and dynamic cell morphometry of living cells with digital holographic microscopy," Opt. Express **13**(23), 9361–9373 (2005).
3. C. J. Mann, L. F. Yu, C. M. Lo, and M. K. Kim, "High-resolution quantitative phase-contrast microscopy by digital holography," Opt. Express **13**(22), 8693–8698 (2005).
4. G. Popescu, T. Ikeda, R. R. Dasari, and M. S. Feld, "Diffraction phase microscopy for quantifying cell structure and dynamics," Opt. Lett. **31**(6), 775–777 (2006).
5. W. Choi, C. Fang-Yen, K. Badizadegan, S. Oh, N. Lue, R. R. Dasari, and M. S. Feld, "Tomographic phase microscopy," Nat. Methods **4**(9), 717–719 (2007).
6. Y. J. Sung, W. Choi, C. Fang-Yen, K. Badizadegan, R. R. Dasari, and M. S. Feld, "Optical diffraction tomography for high resolution live cell imaging," Opt. Express **17**(1), 266–277 (2009).
7. F. Charrière, A. Marian, F. Montfort, J. Kuehn, T. Colomb, E. Cuche, P. Marquet, and C. Depeursinge, "Cell refractive index tomography by digital holographic microscopy," Opt. Lett. **31**(2), 178–180 (2006).
8. B. Rappaz, F. Charrière, C. Depeursinge, P. J. Magistretti, and P. Marquet, "Simultaneous cell morphometry and refractive index measurement with dual-wavelength digital holographic microscopy and dye-enhanced dispersion of perfusion medium," Opt. Lett. **33**(7), 744–746 (2008).
9. G. Popescu, Y. Park, N. Lue, C. Best-Popescu, L. Deflores, R. R. Dasari, M. S. Feld, and K. Badizadegan, "Optical imaging of cell mass and growth dynamics," Am. J. Physiol. Cell Physiol. **295**(2), C538–C544 (2008).

#116663 - $15.00 USD Received 2 Sep 2009; accepted 28 Sep 2009; published 2 Oct 2009

10. Y. Park, M. Diez-Silva, G. Popescu, G. Lykotrafitis, W. Choi, M. S. Feld, and S. Suresh, "Refractive index maps and membrane dynamics of human red blood cells parasitized by Plasmodium falciparum," Proc. Natl. Acad. Sci. U.S.A. **105**(37), 13730–13735 (2008).
11. R. Barer, "Refractometry and interferometry of living cells," J. Opt. Soc. Am. **47**(6), 545–556 (1957).
12. B. S. Chincholi, A. J. Havlik, and R. D. Vold, "Specific refractive index increments of polymer systems at four wavelengths," J. Chem. Eng. Data **19**(2), 148–152 (1974).
13. B. J. Zeskind, C. D. Jordan, W. Timp, L. Trapani, G. Waller, V. Horodincu, D. J. Ehrlich, and P. Matsudaira, "Nucleic acid and protein mass mapping by live-cell deep-ultraviolet microscopy," Nat. Methods **4**(7), 567–569 (2007).
14. A. Pinchuk, "Optical constants and dielectric function of DNA's nucleotides in UV range," J. Quant. Spectrosc. Radiat. Transf. **85**(2), 211–215 (2004).
15. M. Andersen, L. R. Painter, and S. Nir, "Dispersion-Equation and Polarizability of Bovine Serum-Albumin from Measurements of Refractive-Indexes," Biopolymers **13**(6), 1261–1267 (1974).
16. M. Friebel, and M. Meinke, "Determination of the complex refractive index of highly concentrated hemoglobin solutions using transmittance and reflectance measurements," J. Biomed. Opt. **10**(6), 064019–064015 (2005).
17. W. Choi, C. C. Yu, C. Fang-Yen, K. Badizadegan, R. R. Dasari, and M. S. Feld, "Field-based angle-resolved light-scattering study of single live cells," Opt. Lett. **33**(14), 1596–1598 (2008).
18. H. F. Ding, Z. Wang, F. Nguyen, S. A. Boppart, and G. Popescu, "Fourier transform light scattering of inhomogeneous and dynamic structures," Phys. Rev. Lett. **101**(23), 238102 (2008).
19. A. Wax, C. Yang, R. R. Dasari, and M. S. Feld, "Measurement of angular distributions by use of low-coherence interferometry for light-scattering spectroscopy," Opt. Lett. **26**(6), 322–324 (2001).
20. T. Ikeda, G. Popescu, R. R. Dasari, and M. S. Feld, "Hilbert phase microscopy for investigating fast dynamics in transparent systems," Opt. Lett. **30**(10), 1165–1167 (2005).
21. N. Ghosh, P. Buddhiwant, A. Uppal, S. K. Majumder, H. S. Patel, and P. K. Gupta, "Simultaneous determination of size and refractive index of red blood cells by light scattering measurements," Appl. Phys. Lett. **88**(8), 084101 (2006).
22. M. Daimon, and A. Masumura, "Measurement of the refractive index of distilled water from the near-infrared region to the ultraviolet region," Appl. Opt. **46**(18), 3811–3820 (2007).
23. C. M. Stoscheck, and P. D. Murray, "Quantitation of protein," Methods Enzymol. **182**, 50–68 (1990).

1. Introduction

Refractive indices of biomolecules play crucial roles in many optical imaging and microscopy techniques developed for cell biology. Phase contrast and differential interference contrast (DIC) microscopy have long been used to observe unstained live cells by generating contrast from refractive index variations of organelles within cells. This contrast provides fundamental biophysical information about the structure and organization of cells. In recent years, there has been growing interest in developing quantitative phase microscopy (QPM) techniques for cell characterization in both two dimensions and three dimensions [1–7]. Compared to phase contrast and DIC microscopy, QPM enables to obtain quantitative phase information proportional to the optical path length of transparent cells with sub-wavelength accuracy. This leads to the quantitative measurements of physical thickness and refractive index of cells, as well as qualitative study of cellular organization. A few examples of interesting applications include assessment of cellular morphology, measurement of cell dry mass and study of red blood cell dynamics [8–10]. Most of these applications, however, are incapable of distinguishing different molecules present in the cell because measurements are performed in the visible wavelength range far from the resonance absorption wavelengths of most biomolecules. DNA molecules and most proteins have about the same specific refractive index increment α — the physical parameter which directly relates refractive index to molecular concentration C: $n = n_0 + \alpha C$, where n_0 and n are the index of the solvent and the solution, respectively. Typical value of α for proteins is around 0.18-0.19 mL/g [11] whereas for DNA molecules, it is around 0.17-0.18 mL/g [12]. Also, the refractive index dispersion of these molecules (the dependence of α on wavelength) is almost the same. As a result, it is very difficult to separately quantify them inside individual cells, which is an important issue in biology.

A straightforward solution is to make measurements in the ultraviolet (UV) region. As is well known, protein and DNA have distinct absorption spectra in the deep UV and they show substantially different refractive index dispersion near their absorption peaks. We note that absorption based microscopy technique has already demonstrated separate quantification of

#116663 - $15.00 USD Received 2 Sep 2009; accepted 28 Sep 2009; published 2 Oct 2009

DNA and proteins [13]. However, imaging at the absorption peak of protein and DNA, necessary to maximize the detection sensitivity, presents great challenges in controlling photodamage to the living cell. On the other hand, the refractive index dispersion is significant even tens of nanometers away from the absorption peak. Therefore, it is possible to separate them in the QPM while reducing the photodamage from strong absorption. However, very limited literature reports the refractive index measurement of biomolecules in the deep UV. Although the Kramers-Kronig relationship can be used to derive the refractive index dispersion from the measured absorption spectrum [14], the difficulty in obtaining absorption spectrum below 200 nm prevents accurate calculation of the refractive index. While commercial refractometers based on total internal reflection can routinely achieve greater accuracy than 0.0001, none exists for measurement in the UV regime. Index of refraction can also be measured by the reflectance method [15,16], but it is not accurate enough to measure dispersion shape near the absorption peak.

In this report, we propose a refractive index measurement method based on QPM. The light scattering distribution is obtained by taking the Fourier transform of the E-field image (both amplitude and phase images) taken by QPM [17,18]. For a single microsphere immersed in a transparent medium, fitting the measured angular scattering spectrum with Mie scattering theory can determine the size of the microsphere and the refractive index ratio between the sphere and the immersion medium. We call this approach the field-based light scattering spectroscopy (FLSS) approach. This method has several advantages over the traditional reflectance or refraction based method. First, it uses the same setup as QPM, and therefore is readily adaptable to microscope based techniques. Second, it is not limited to solution measurement, but could in principle measure any spherical structures including spheroidal cells. We note that conventional light scattering spectroscopy also utilizes least square fitting of the scattering spectrum with Mie theory with large numbers of beads in the field of view [19]. Our approach, however, presents enough sensitivity to detect scattering distribution from a single bead and thus exclude the effect of sample size distribution. With this FLSS method, we have measured the refractive index dispersion of SiO_2 spheres and protein solutions in the deep UV region (λ = 260 - 315 nm). Specific refractive index increment is obtained by linear regression of refractive indices on protein concentrations. The precision of refractive index determination is typically ≤0.001 for SiO_2 spheres and ≤0.002 for protein solutions. Accuracy of refractive index determination is better than 0.003.

2. Experimental setup

The design of the UV quantitative phase microscope is described in Fig. 1. The principle of measurement is based on diffraction phase microscopy, which has the advantages of common path geometry and single shot measurement [4]. The UV light source is a frequency-doubled tunable optical parametric amplifier (Coherent OPA 9400) pumped by a femtosecond amplified Ti: Sapphire laser system (Coherent RegA 9000 seeded by Coherent Mira 900). The wavelength tuning range is from 250 to 350 nm, which covers the first protein absorption peak located around 280 nm. Total output power is around 1-2 mW. Residual visible light present after BBO crystal, used for frequency doubling, is filtered out using a glass filter (Thorlabs, FGUV5). The UV laser beam is loosely focused onto the sample with a 25 cm focal length lens and the spot diameter is around 30 μm. The sample, typically microspheres immersed in water or protein solution, is sandwiched between two quartz coverslips (SPI Supplies) and located at the beam waist of the UV laser. It is imaged by a glycerol immersion objective (Leitz 100 × , NA = 1.20) and a 15 cm focal length tube lens. A diffraction grating (Edmund Optics, 100 lines/mm Ronchi Grating) is placed at the intermediate image plane IP1. Two fused silica lenses with focal lengths of 7.5 cm and 20 cm form a telescope which relays the magnified image onto a CCD camera (Photometric Sensys, 768 × 512 pixels with 9 × 9 μm^2 pixel size) positioned at the second image plane IP2. The overall magnification from sample plane to CCD plane is 240. At the intermediate Fourier plane FP, a custom cut pinhole

#116663 - $15.00 USD Received 2 Sep 2009; accepted 28 Sep 2009; published 2 Oct 2009

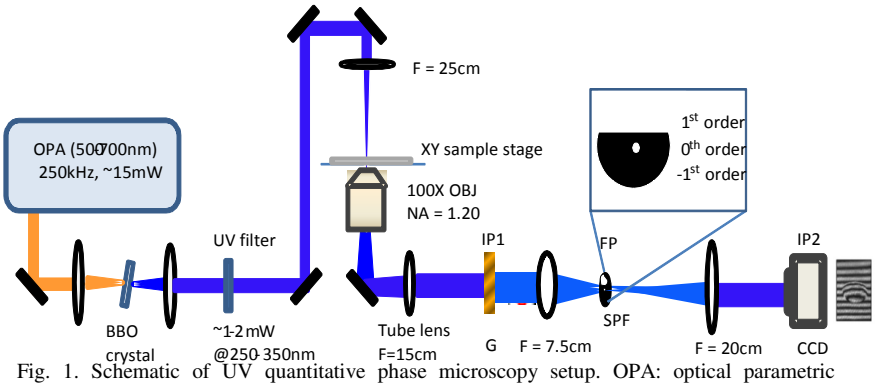

Fig. 1. Schematic of UV quantitative phase microscopy setup. OPA: optical parametric amplifier, BBO: β-Barium Borate, OBJ: objective, G: grating, IP1: image plane 1, FP: Fourier plane, SPF: spatial filter. IP2: image plane 2.

(Edmund Optics, d = 12 μm) is placed. Two beams (0th and the 1st diffraction order) are isolated in order to be used as the reference and sample fields, respectively. The 0th order beam is spatially filtered with the pinhole to provide a pseudo-plane wave at the CCD plane, while the 1st order beam carrying the sample information is unperturbed and pass through completely. The sample and reference fields interfere at the CCD plane and generate spatial interference fringes, which can be Hilbert transformed to provide the complex E-field image of the sample.

3. Data analysis

Data analysis is performed in two steps: (1) converting quantitative phase images to angular scattering spectra, and (2) least square fitting of the measured scattering distribution using Mie scattering theory to determine size and refractive index.

The first step is illustrated in Fig. 2. First, an interference image of a sample (a single SiO_2 sphere immersed in water, Fig. 2a) is measured with the CCD camera, and a back ground image (no sample in the field of view, Fig. 2b) is taken. The background image is used to compensate for the nonuniform illumination caused by defects in the optics and dust in the optical beam path. Using Hilbert transform [20], complex E-field images (both the amplitude and the phase) of the sample and background are acquired. The sample E-field is then normalized by the background E-field (Fig. 2c-d). Next, the complex E-field at the Fourier plane is derived by applying 2D Fourier transform to the complex E-field image at the image plane. The absolute square of the resulting E-field gives the scattering intensity distribution (Fig. 2e) [17,18]. This pattern is equivalent to direct intensity measurement in the Fourier plane that is traditionally used in light scattering studies. As can be seen, there is a strong DC component in the center because most of the incident photons are not scattered, but transmitted due to the weak refractive index contrast of the sample to the medium. From the intensity scattering pattern, the angular scattering spectrum can be obtained through azimuthal averaging (Fig. 2f). Oscillations from spherical scatterers as predicted by Mie scattering theory can be easily seen up to 40 degrees. At higher angles, residual background noise, shot noise and camera readout noise start to dominate. As a general rule, the period of the oscillation determines the size of the sphere, and the position of the intensity maxima determines the refractive index of the sphere [21].

#116663 - $15.00 USD Received 2 Sep 2009; accepted 28 Sep 2009; published 2 Oct 2009

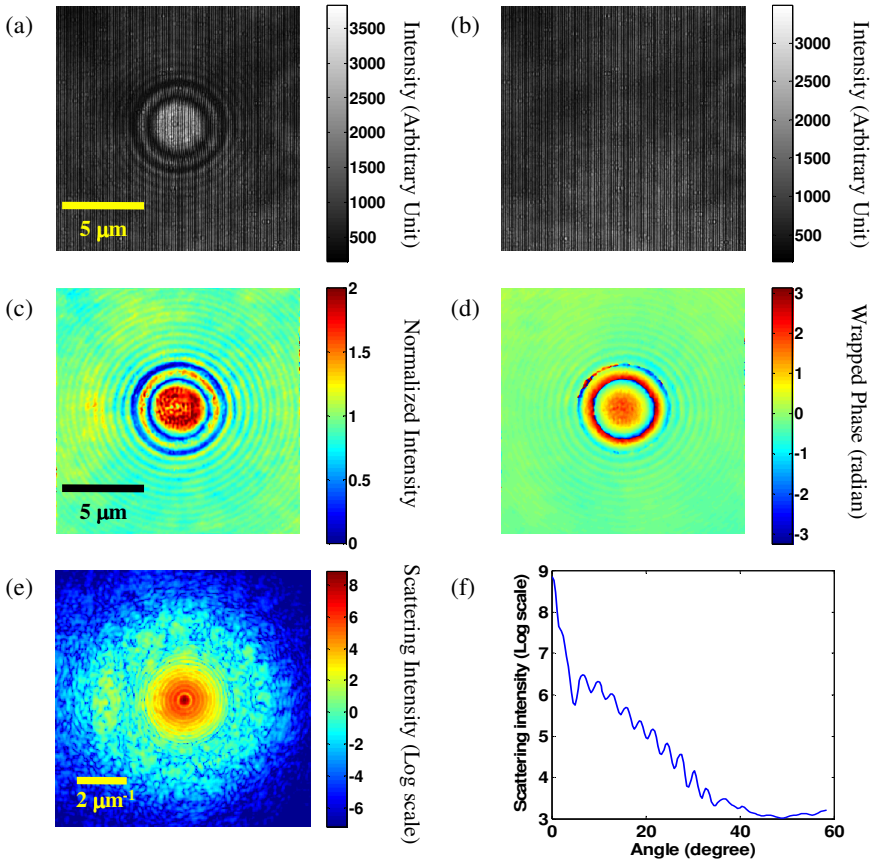

Fig. 2. (a) interference image of a SiO_2 sphere immersed in water and (b) background captured by the CCD at 315 nm; (c) normalized amplitude and (d) phase image of the same sphere; (e) intensity scattering pattern in logarithm scale derived from Fourier transform of the E-field in the image plane; (f) angular scattering spectrum obtained through azimuthal averaging of (e).

Measuring in the image plane instead of the Fourier plane has an advantage in sensitivity, i.e. utilizing the full dynamic range of the camera. For a weakly scattering sample the intensity distribution in the image plane is much more uniform, and therefore a much larger dynamic range can be obtained with the same camera [17]. As can be seen in Fig. 2f, the angular scattering intensity distribution usually spans more than five orders of magnitude from 0 to 60 degrees, which cannot be covered if scattering intensity is directly measured in the Fourier plane in a single exposure. As a result, measurement in the image plane can be easily performed on a single sphere while measurement in the Fourier plane is usually done with many spheres to increase signal-to-noise ratio. Considering the variation of size (and possibly refractive index) in spheres, fitting for a single sphere will yield more accurate results compared to many spheres.

The second step is to determine the size and refractive index of the sphere from the measured angular scattering distribution. The phase function of light scattering from an ideal spherical object is computed based on Mie theory as a function of diameter and refractive index of spheres with size increment of 0.01 μm and refractive index increment of 0.001. Refractive index of medium, water in this case, is determined using literature value [22]. The experimental angular scattering spectrum is then compared to theoretical spectra. The χ^2 residuals are calculated for each size and refractive index of phase function. In this experiment, the scattering angular range from 3° to 35° is used to compute χ^2. It is found that

#116663 - $15.00 USD Received 2 Sep 2009; accepted 28 Sep 2009; published 2 Oct 2009

the slope of angular scattering intensity changes with the focal position. To minimize this effect, a linear slope is subtracted from both measured and calculated scattering spectra before taking their difference. The inverse of χ^2 is then normalized and plotted in Fig. 3a as an error map. $\chi^2 = 1$ corresponds to minimum error and predicts the size and refractive index of the sphere. For the particular sphere used in this measurement, the size and the refractive index at 315 nm were determined to be 4.69 μm and 1.456, respectively. The experimental angular scattering distribution is in excellent agreement with the fitting as shown in Fig. 3b.

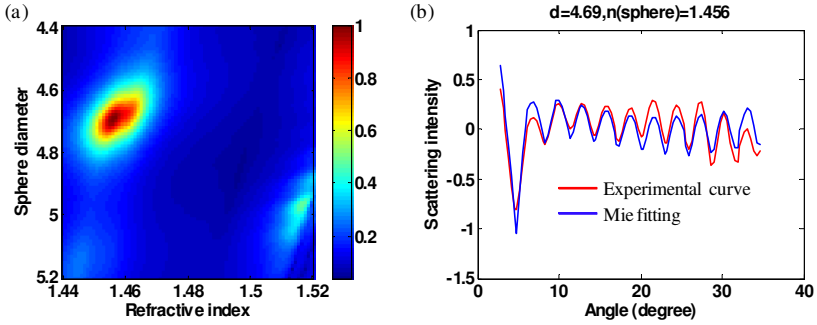

Fig. 3. (a) Normalized 1/χ2 map of the difference between experimental scattering spectrum and that of Mie scattering as a function of sphere size and index of refraction. (b) Comparison of experimental scattering spectrum with the predicted scattering spectrum (Mie theory).

4. Experimental results

In order to determine the refractive index of an arbitrary solution of interest, we first determined the average refractive index of SiO_2 spheres immersed in water as described in the previous section. For each wavelength, typically 6-8 spheres were imaged and analyzed. Once the refractive index of SiO_2 spheres was determined for each wavelength, similar measurements were performed on spheres immersed in the solution of interest, bovine serum albumin (BSA) solutions in our study. In creating the Mie error map, phase functions were computed as we vary the refractive index of the medium while fixing that of the SiO_2 sphere with the previously measured value. We then found the specific size of sphere and index of solution which provide the least square residual χ^2. By doing so, the refractive indices of protein solutions were determined in the same way as that of SiO_2 spheres.

SiO_2 spheres with 5 μm size and 10-15% size variation were purchased from Polysciences Inc. SiO_2 spheres were chosen instead of widely used polystyrene spheres because polystyrene has strong UV absorption which complicates Mie scattering calculation. BSA solutions (Sigma-Aldrich) were prepared at five different concentrations from 0.5 g/mL to 0.25 g/mL. We first measured the refractive index of SiO_2 and BSA solutions at 633 nm. The results were compared to that measured with a commercial refractometer to evaluate the accuracy of our measurements. After that, the refractive index dispersion of SiO_2 sphere and BSA solutions were determined in the UV from 260 to 315 nm. For each wavelength, the specific refractive index increment of BSA was calculated.

4.1 Validation of FLSS refractive index measurement method in the visible

To evaluate the accuracy of our method, we compared our measurements with those of a commercial refractometer. Since the commercial refractometer supports only visible wavelengths, we also made measurements at visible wavelength (633nm, He-Ne laser). With the FLSS method the refractive index of SiO_2 spheres was first determined at 633 nm to be 1.4319 ± 0.0018 and the size was measured to be 4.727 ± 0.025μm. These measurements are consistent with the manufacturer's specifications of refractive index 1.43-1.46 and size 5 μm. We used the refractive index of sphere 1.4319 in the Mie scattering calculation and

#116663 - $15.00 USD Received 2 Sep 2009; accepted 28 Sep 2009; published 2 Oct 2009

determined the refractive index of BSA solutions at different concentrations. The refractive indices of BSA solutions were also measured using a commercial digital refractometer (Cole-Parmer) and the results compared to that determined by the FLSS method. Figure 4 shows the refractive index increments of protein solutions over water at different concentrations for both methods. A linear relationship is observed, as expected. The accuracy of our FLSS method, determined from the difference in both measurement, is better than 0.003. The specific refractive index increment α was obtained by linear fitting of the measured refractive indices with respect to concentrations. α determined by the FLSS method is 0.188 mL/g and has only ~1% error from that of refractometer measurement, therefore confirming the accuracy of the FLSS method.

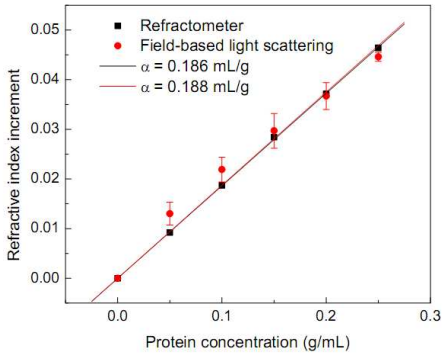

Fig. 4. Comparison of refractive index increments over water determined using the FLSS method (red dots) at 633 nm to that measured by a commercial refractometer (black squares). The red and black lines are the corresponding linear fits of refractive index increments to BSA concentration; the slopes represent specific refractive index increments α. The error bars represent standard deviations.

4.2 Refractive index dispersion of SiO_2 spheres and protein solutions in the UV

After establishing the accuracy of our FLSS method for visible wavelengths, we determined the refractive index dispersion of SiO_2 spheres at several wavelengths in the UV region by immersing them in water, the dispersion of which has previously been measured [22]. The

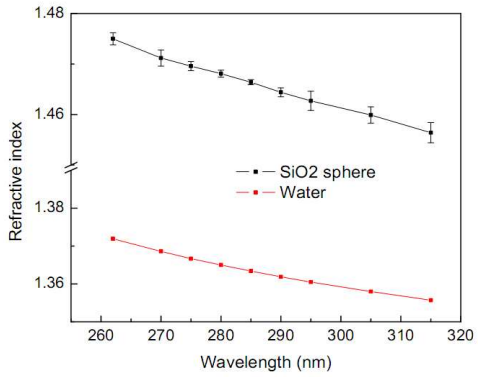

Fig. 5. Refractive index dispersion of SiO2 sphere determined by the FLSS method (black squares) and water obtained from reference [22] (red dots) in the UV range. The error bars for SiO2 sphere are the standard deviations of 6-8 measurements at each wavelength.

results are shown in Fig. 5. SiO_2 spheres exhibit very low dispersion, similar to water. Their refractive index in deep UV is substantially higher than that in the visible by 0.03-0.05. The

#116663 - $15.00 USD Received 2 Sep 2009; accepted 28 Sep 2009; published 2 Oct 2009

precision of refractive index determination can be reflected by the standard deviation of multiple measurements, which is typically <0.002.

After the refractive index dispersion of SiO_2 spheres is obtained, the same approach as discussed in section 4.1 can be applied to BSA solutions at various concentrations to extract specific refractive index increments of BSA in the UV range. Figure 6a shows the refractive index measurement at 315 nm. Here the precision is higher than that at 633 nm, mostly because the number of oscillations in the angular scattering spectrum is about twice larger in the UV range than in the visible and therefore fitting accuracy is enhanced. The specific refractive index increment α is 0.213 ± 0.005 mL/g. Error is determined by the error of linear regression. α is about 0.025 mL/g higher than that in the visible range. Figure 6b shows α as a function of wavelength, or the refractive index dispersion, at several UV wavelengths. The corresponding absorption curve measured with a UV-Vis Spectrophotometer (Shimadzu, UV-2401PC) is also displayed in terms of optical density (O.D.) for 0.25 g/mL BSA solution diluted by 400 times. A dispersive shape of refractive index is observed near the absorption peak at 280 nm with a local maximum α = 0.288 mL/g at 285 nm. Further sharp increase of refractive index below 280 nm is caused by another strong resonance at 205 nm [23]. Typical precision in determining α is <0.01 mL/g. At wavelengths below 280 nm, the strong absorption from BSA solution and the low camera sensitivity lead to very low fringe contrast in QPM. Only concentrations from 0.05 g/mL to 0.15 g/mL were measured. Therefore, the error in determining α is much higher at wavelengths shorter than 280 nm. We observed 35% increases in α from 315 to 285 nm. The corresponding refractive index increase is 0.0227 for protein solution at a concentration of 0.2 g/mL (typical concentration of protein in cell cytoplasm), whereas it is only 0.0077 for water.

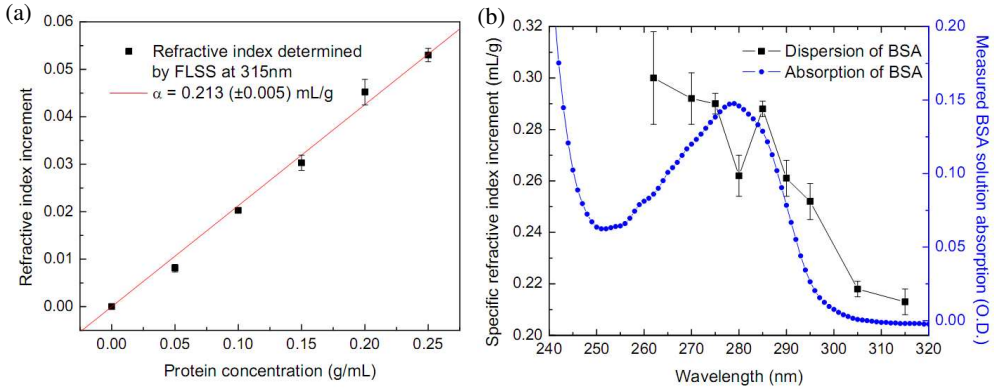

Fig. 6. (a) Specific refractive index increments determined by the FLSS method at 315 nm through linear regression of refractive indices of protein solutions on protein concentrations. The error bar at each measurement point is the standard deviation of 6-8 measurements. (b) Refractive index dispersion of protein solution determined by the FLSS method (black squares) in the UV range. The error bar corresponds to linear regression error at each wavelength. Absorption of 0.25 g/mL BSA solution diluted by 400 times is also displayed (blue dots).

5. Conclusion

We have proposed and demonstrated a refractive index measurement method using field-based light scattering. It is fully compatible with existing quantitative phase microscopy setup and only involves modification of the data analysis method. Therefore, refractive index calibration and phase microscopy can be performed simultaneously. This method also has the advantage of much larger dynamic range compared to traditional light scattering methods. The accuracy of our refractive index measurements were evaluated in the visible by comparing to standard commercial refractometer measurements. For single concentration measurement, the refractive index error is <0.003. For specific refractive index increment, the error is ~1%.

#116663 - $15.00 USD Received 2 Sep 2009; accepted 28 Sep 2009; published 2 Oct 2009

With this new FLSS refractive index measurement method, we determined the refractive index dispersion of SiO_2 sphere and protein solutions in the deep UV region from 260 nm to 315 nm. Typical precision of refractive index measurement is ≤0.002. Precision of specific refractive index increment determination is typically ≤0.01 mL/g or 5%.

It is observed that SiO_2 spheres have a very low dispersion, similar to water. Increase in refractive index from visible to deep UV is 0.03-0.05. Within the measured UV range, only small monotonic increase in refractive index is observed with decreasing wavelength. For BSA solutions, a characteristic dispersive shape around the protein absorption peak in refractive index/wavelength plot is observed. Further increase below the absorption peak can be attributed to another strong absorption at 205 nm. The specific refractive index increment increases by 35% from 315 nm to 285 nm. Assuming a protein concentration of 0.2 g/mL, the refractive index increases by 0.0227, while for water it is only about one third of that increase. Since DNA also has distinctive absorption spectra in the deep UV range, it is possible that the difference in dispersion between protein and DNA will enable separate quantifications based on quantitative phase imaging at different wavelengths. In the future, we will improve our quantitative phase microscope system, e.g. using a better UV transmitting objective and UV sensitive camera to improve the detection sensitivity and minimize photodamage, and ultimately to study live cells.

Acknowledgements

This work was funded by the National Center for Research Resources of the National Institutes of Health (P41-RR02594-18), the National Science Foundation (DBI-0754339), and

Hamamatsu Corporation. YKP was supported by Samsung Scholarship and Whitaker Health Science Fellowship.

#116663 - $15.00 USD Received 2 Sep 2009; accepted 28 Sep 2009; published 2 Oct 2009